https://doi.org/10.5194/essd-2024-545
Preprint. Discussion started: 13 January 2025

Open Access Earth System Science Data Discussions

Global air-sea heat and freshwater fluxes constrained by ocean observations

Taimoor Sohail[1,2] and Jan David Zika[1,2,3]

[1]School of Mathematics and Statistics, University of New South Wales, Sydney, Australia
[2]Australian Center for Excellence in Antarctic Science, University of New South Wales, Sydney, Australia
[3]UNSW Data Science Hub (uDASH), University of New South Wales, Sydney, Australia

Correspondence: Taimoor Sohail (t.sohail@unsw.edu.au)

Abstract. A substantial portion of the transport of heat and freshwater in the climate system occurs through the ocean. Heat and fresh water enter the ocean as air-sea fluxes, which are typically estimated based on observationally constrained 'reanalyses' of the atmosphere. However, these estimates are uncertain, with broad differences in space and time between different products, and do not align with estimates of integrated ocean temperature and salinity. As a result, inferred global heat and freshwater transport, including transport trends, remain unclear. In this work, we use a novel water mass-based inverse modelling method, the Optimal Transformation Method (OTM), to reconcile reanalysis-based changes in surface heat and freshwater fluxes with changes in observed ocean temperature and salinity. We present estimates of air-sea surface fluxes since the 1970s, derived from reanalysis products ERA5, JRA-55 and COREv2, which are adjusted to be physically consistent with observation-based 3D ocean temperature and salinity products EN4 and IAP. OTM adjusts air-sea surface fluxes in a consistent manner, thereby also enabling estimation of meridional heat and freshwater transports. Inferred mean meridional heat transport is relatively consistent, and aligns with independent ocean transport observations and the spread of estimates from historical reconstructions from the 6th Climate Model Intercomparison Project. Mean freshwater transport and trends in both heat and freshwater transport are less consistent. Either a narrowing of the range of estimates provided by reanalyses and/or additional constraints to OTM (in addition to the thermodynamic constraints currently provided) are therefore still needed.

1 Introduction

A vast proportion of excess heat in the atmosphere is absorbed by the global ocean (Schuckmann et al., 2020). In addition, a substantial amount of freshwater enters the ocean through the atmospheric limb of the water cycle (Trenberth et al., 2007). The exchange of heat and freshwater from the atmosphere to the ocean leaves a signature in ocean temperature and salinity (Durack et al., 2012; Skliris et al., 2016; Sohail et al., 2022; Zika and Sohail, 2023). Ocean currents and mixing then redistribute changes in temperature and salinity, often resulting in tracer property changes far from the locations where air-sea exchanges are largest. (Zika et al., 2021; Todd et al., 2020; Basinski-Ferris and Zanna, 2023) The absorption of heat and freshwater by the ocean, and the subsequent redistribution of these tracers, is essential to our global climate, regulating global temperatures and ensuring the viability of life on earth (Bryan, 1982; Stocker, 2013).

https://doi.org/10.5194/essd-2024-545
Preprint. Discussion started: 13 January 2025

Open Access Earth System Science Data Discussions

In order to understand fundamental changes to our global ocean, it is important to ensure we have a rich and accurate set of estimates of air-sea heat and freshwater exchanges and ocean heat and salt content. A set of well-defined ocean tracer properties and air-sea fluxes, enables the inference of meridional tracer transports, which are the "engine" of our global climate (Valdivieso et al., 2014; Trenberth et al., 2019). However, current best guesses of air-sea heat and fluxes, and the subsequent impact on ocean heat content and transport, remains uncertain (Trenberth and Caron, 2001; Valdivieso et al., 2017; Trenberth and Fasullo, 2017; Grist et al., 2016). Air-sea heat and freshwater flux products have large global flux biases compared to observed ocean tracer content changes, and tend to disagree over broad spatial and time-scales (Valdivieso et al., 2017; Bentamy et al., 2017; Balmaseda et al., 2015; Trenberth, 2010). Given the key role the ocean plays in exchanging atmospheric heat and freshwater and redistributing it around the planet, it is essential to constrain these long-term air-sea tracer fluxes such that they match observations of ocean tracer content.

In the past, 'inverse modelling' has been used to obtain physically permissive estimates of meridional heat and freshwater transports and/or air-sea tracer fluxes (Wunsch, 1978; Zanna et al., 2019; Groeskamp et al., 2019; Talley, 2008; McDonagh et al., 2015; Li et al., 2021; Arumí-Planas et al., 2024). For instance, Trenberth et al. (2019) inferred meridional heat transport as the residual between air-sea heat fluxes and vertically integrated ocean heat content, adding a spatially uniform adjustment to surface fluxes to ensure global closure of the heat budget. Roberts et al. (2017) used a linear Kalman filtering algorithm to combine atmospheric reanalysis-based air-sea fluxes with ocean observations and close the global ocean heat budget. Valdivieso et al. (2014), on the other hand, used an ocean-sea ice model, forced by surface forcings from an atmospheric reanalysis product, to produce an internally consistent set of air-sea freshwater fluxes and freshwater transports via data assimilation. However, many of these inverse modelling efforts rely on assumptions that ocean dynamics are linear, that ocean circulation is steady or dominated by geostrophic dynamics, or that surface air-sea fluxes have a constant (or no) bias everywhere.

Here, we produce a set of air-sea flux fields that have been adjusted to match observed ocean tracer changes using a novel inverse method (termed the *Optimal Transformation Method*, OTM). OTM combines surface air-sea heat and freshwater fluxes and observed ocean tracer changes to determine a physics-constrained estimate of ocean tracer transport. OTM achieves this by leveraging the uniquely constrained nature of oceanic distribution changes in phase space - specifically temperature-salinity coordinates. Using OTM, we present a series of physically-consistent surface heat and freshwater fluxes, modified from ERA5, JRA-55 and COREv2 surface flux fields, averaged from 1979 to 2014 (1979 to 2006 for COREv2). These adjusted surface air-sea flux fields are consistent with time-mean global (and, as much as possible, basin-scale) tracer properties in the EN4.2.2 and IAPv3 gridded ocean observational data products over the same time period. In section 2, we describe the Optimal Transformation Method in further detail, and in section 3 we outline the datasets used in this study. In section 4, we explore the adjusted air-sea flux data sets, both in terms of their contribution to the closed global heat and salt budgets, as well as the resulting estimates of meridional heat and freshwater transports. In section 5, we highlight the key areas of improvement, both for OTM and our surface air-sea flux fields, and summarise our main findings in section 6.

https://doi.org/10.5194/essd-2024-545
Preprint. Discussion started: 13 January 2025

Open Access Earth System Science Data Discussions

2 Theory

In this work, we use the *Optimal Transformation Method*, OTM, to explain observed ocean water mass changes with a combination of ocean mixing, circulation changes and air-sea flux changes (the latter of which are minimally adjusted to ensure physical consistency). The Optimal Transformation Method leverages the fact that changes to a given volumetric distribution in temperature-salinity (T-S) space are governed by physical constraints (Zika and Sohail, 2023). Specifically, while surface heat fluxes can move water masses in any direction in T-S space, mixing *must* be a linear, convergent and irrotational combination of two or more water masses (see Nurser et al. for a formal proof). Thus, if a known surface heat and freshwater flux transforms a set of water masses in T-S space, mixing can be inferred as a physically-constrained combination of these water masses after they have been transformed by the surface fluxes.

The inputs to OTM are an observed volumetric T-S distribution of the ocean at time t_0 and t_1, and an estimate of the surface heat and freshwater flux field between t_0 and t_1. If an observed set of i water masses at t_0 with concentrations $\mathbf{C}_{0,i}$ and volumes $\mathbf{V}_{0,i}$ become a set of j water masses at t_1 with concentrations $\mathbf{C}_{0,i}$ and volumes $\mathbf{V}_{1,j}$, the final tracer concentration can be expressed in terms of a transformation matrix, with elements g_{ij}, and the surface air-sea fluxes that modify the early water masses as they become the later water masses, $\mathbf{Q}_{ij}$:

$$\mathbf{V}_{1,j} = \sum_{i=1}^{N} g_{ij} \left(\mathbf{V}_{0,i} + \mathbf{Q}_{ij} \right). \tag{1}$$

The surface air-sea fluxes are further decomposed into 'prior' and 'adjustment' components such that $\mathbf{Q}_{ij} = \mathbf{Q}_{ij}^{prior} + \mathbf{Q}_{ij}^{adjust}$, where the former is based on atmospheric reanalysis and the latter is solved for using constrained linear optimization.

The volumetric distribution of the ocean is coarsened using a *Binary Space Partitioning* (BSP) algorithm (see Sohail et al. (2023); Zika and Sohail (2023) for more information) into N discrete water masses spread over different ocean basins. The surface air-sea heat and freshwater fluxes are also integrated over a geographical region corresponding to these N water masses, defined by time-varying spatial masks Ω_i or Ω_j, such that $\mathbf{Q}_i^{prior} = \frac{1}{V_{0,i}(t_1 - t_0)} \int_{t_0}^{t_1} \iint \Omega_i(x,y,0,t) \mathbf{q}(x,y,t) dx dy dt$, where $\mathbf{q}(x,y,t)$ is the two-dimensional, time-varying surface air-sea flux field representing combined freshwater and heat fluxes.

OTM derives a solution for a transformation matrix, g_{ij} which optimally explains how the early water masses at time t_0, once modified by the estimated air sea heat and fresh water fluxes, are redistributed and mixed together to form the late water masses at time t_1. Although both the ocean observational analysis-based water mass distributions and the atmospheric reanalysis-based surface air-sea fluxes are subject to substantial uncertainty, because the air sea fluxes exhibit a larger spread, we choose to find a solution for g_{ij} which minimises the necessary adjustment to the air-sea flux, $\mathbf{Q}_{ij}^{adjust}$. To do this, we solve a constrained (conic) linear optimisation problem with the following constraints:

https://doi.org/10.5194/essd-2024-545
Preprint. Discussion started: 13 January 2025

Open Access Earth System Science Data Discussions

$$0 \leq g_{ij} \leq 1; \tag{2}$$

$$V_{1,j} = \sum_{i=1}^{N} V_{0,i} g_{ij}; \tag{3}$$

$$V_{0,i} = \sum_{j=1}^{N} V_{1,j} g_{ij}; \tag{4}$$

$$\mathbf{C}_{1,j} V_{1,j} = \sum_{i=1}^{N} \mathbf{C}_{0,i} V_{0,i} g_{ij} \text{ where } A_j = 0; \tag{5}$$

$$g_{ij} = 0 \text{ if } \Omega_i \text{ and } \Omega_j \text{ are not in the same or adjacent regions,} \tag{6}$$

where Ω_i and Ω_j are masks corresponding to the geographical location of a given water mass (Fig.1) and $A_i$and A_j are the outcrop area of the water masses. Under the above constraints, we minimise the cost function:

$$[\text{Cost function}] = \sum_{j=1}^{N} \left|\left| \mathbf{w}_j \left(\sum_{i=1}^{N} V_{0,i} g_{ij} \left(\mathbf{C}_{0,i} + \mathbf{Q}_{ij}^{prior} \right) - V_{1,j} \mathbf{C}_{1,j} \right) \right|\right|^2, \tag{7}$$

where the weights are defined as $\mathbf{w}_j = \left[\frac{5\times10^4}{\text{RMSD(TV)}}, \frac{5\times10^4}{\text{RMSD(SV)}} \right]$, and RMSD is the inter-product root-mean-squared difference in surface fluxes. The time-mean squared difference, MSD is calculated as:

$$\text{MSD}_{12} = \frac{1}{T} \sum_{t=1}^{T} \left(\mathbf{q}_1(x,y,t) - \mathbf{q}_2(x,y,t) \right)^2, \tag{8}$$

where 1 and 2 represent the two reanalysis products over which the difference is taken. The RMSD is then calculated as the square root of the MSD averaged over all reanalysis pairs, and is expressed as an equivalent heat or salt content with units of °Cm^3 or gm^3/kg, respectively. To avoid setting an infinite weight when RMSD$= 0$, we set a relatively small value, RMSD$[\text{RMSD} = 0] = 500$ for both RMSD(TV) and RMSD(SV).

Using the python-based linear optimization package *cvxpy* with solver *MOSEK*, we find the transport matrix g_{ij} which satisfies Eqs. 2 to 5 and minimises Eq. 7 between some 'early' and 'late' period. Since the cost is never exactly zero, g_{ij} does not perfectly transform the early water masses into the late water masses. The 'adjustment', or 'correction' term, $\mathbf{Q}_{ij}^{adjust}$, comes out of the optimization as the amount of heat and fresh water required to affect the final transformation to the exact 'late' water masses. In practise, we do not distinguish between adjustments along particular paths for every early water mass i and late water mass j and simply determine one adjustment for each late water mass j. So, $\mathbf{Q}_{ij}^{adjust}$ simply becomes $\mathbf{Q}_{j}^{adjust}$.

We thus diagnose the 'correction' needed to modify the 'priors' (i.e. the set of known air-sea heat fluxes) such that they may be reconciled with the observed volumetric changes to the ocean. This optimisation is repeated over a series of rolling, adjacent time windows, such that the tendency in the transformation vector g_{ij} and adjustment $\mathbf{Q}_{i}^{adjust}$ may be obtained. We transform the air-sea heat flux adjustment, $\mathbf{Q}_{i}^{adjust}$, from T-S space to geographical space by homogenizing $\mathbf{Q}_{j}^{adjust}$ onto the

https://doi.org/10.5194/essd-2024-545
Preprint. Discussion started: 13 January 2025


Open Access Earth System Science Data Discussions

geographical outcrop locations of the N water masses used in the study. This homogenized surface flux adjustment represents the closest that the method, with its coarsened water masses, can get to the 'true' adjusted geographical distribution of the air-sea fluxes. The meridional heat transport as a function of latitude is then diagnosed by subtracting the (adjusted) air-sea heat flux field from the vertically-integrated ocean heat content change and integrating in longitude.

Trenberth et al. (2019) estimated a spatially uniform adjustment to close the global heat budget. With OTM, we go one step further by ensuring the adjusted air-sea fluxes can plausibly describe the changing distribution of water masses in the world ocean. Our method does not rely on any specific numerical model or sub-grid physics prescribed by such a model. Instead, OTM relies only on the fundamental laws governing mixing between water masses. More details on the OTM algorithm may be found in Zika and Sohail (2023), where a validation of OTM is presented for a climate model with closed heat and freshwater budgets, and time-mean meridional heat and freshwater transports are diagnosed.

3 Data

Gridded monthly-averaged temperature (T) and salinity (S) observations (with a 1x1° horizontal resolution) from January 1979 to December 2014 (inclusive) are used to estimate the early and late volume distributions $V_{1,i}$ and $V_{2,j}$ (density is assumed constant so volume is proportional to mass). We use two observational data sets - EN4.2.2 (Good et al., 2013), and a composite observational product which combines IAP gridded data (Cheng and Zhu, 2016; Cheng et al., 2020) above 2000m depth with EN4 data below 2000m depth (the 'IAP composite' data set). Using the Binary Space Partitioning algorithm described in section 2, the volumetric distribution from these observational data sets is coarsened in T-S space into 144 water masses spread across 9 ocean basins which vary in both space and time (see Figure 1 for the time-mean T and S bounds of said water masses in EN4). The T and S bounds of the 144 water masses in the IAP composite data set are shown in Figure S1 of the Supplementary Information.

Gridded monthly-averaged atmosphere/ocean reanalysis products supply the 'prior' surface heat and freshwater flux fields for this analysis. The air-sea fluxes are integrated over the outcrop location of the water masses as defined by BSP, and converted to an equivalent T and S change which modifies the initial volumetric distribution in T-S space. In this analysis, we source air-sea heat and freshwater fluxes from three reanalysis products - ERA5 (Hersbach et al., 2020), JRA-55 (Kobayashi et al., 2015) and COREv2 (Large and Yeager, 2009), the latter being an ocean/atmosphere reanalysis product. These air-sea flux products are chosen because, on average, they exhibit different heat flux biases relative to ocean observations; ERA5 fluxes too much heat into the ocean, JRA-55 cools the ocean too much, and COREv2 is biased warm, though not by as much as ERA5. Figure 2 shows the cumulative global heat and freshwater content changes implied by reanalysis products compared with the observations.

Monthly-averaged data from January 1979 to December 2014 is used for ERA5 and JRA-55, while data from January 1979 to December 2006 is used for COREv2. For the ERA5 and JRA-55 reanalyses, we repeat the optimisation over 6-year rolling windows from 1979-1985 to 2008-2014 (e.g., t_0 =1979-1985 and t_1 =1985-1991; t_0 =1985-1991 and t_1 =1991-1997, etc.). Thus, for ERA5 and JRA-55, we obtain five values for g_{ij} from OTM, which represent the transport necessary to transform

https://doi.org/10.5194/essd-2024-545
Preprint. Discussion started: 13 January 2025

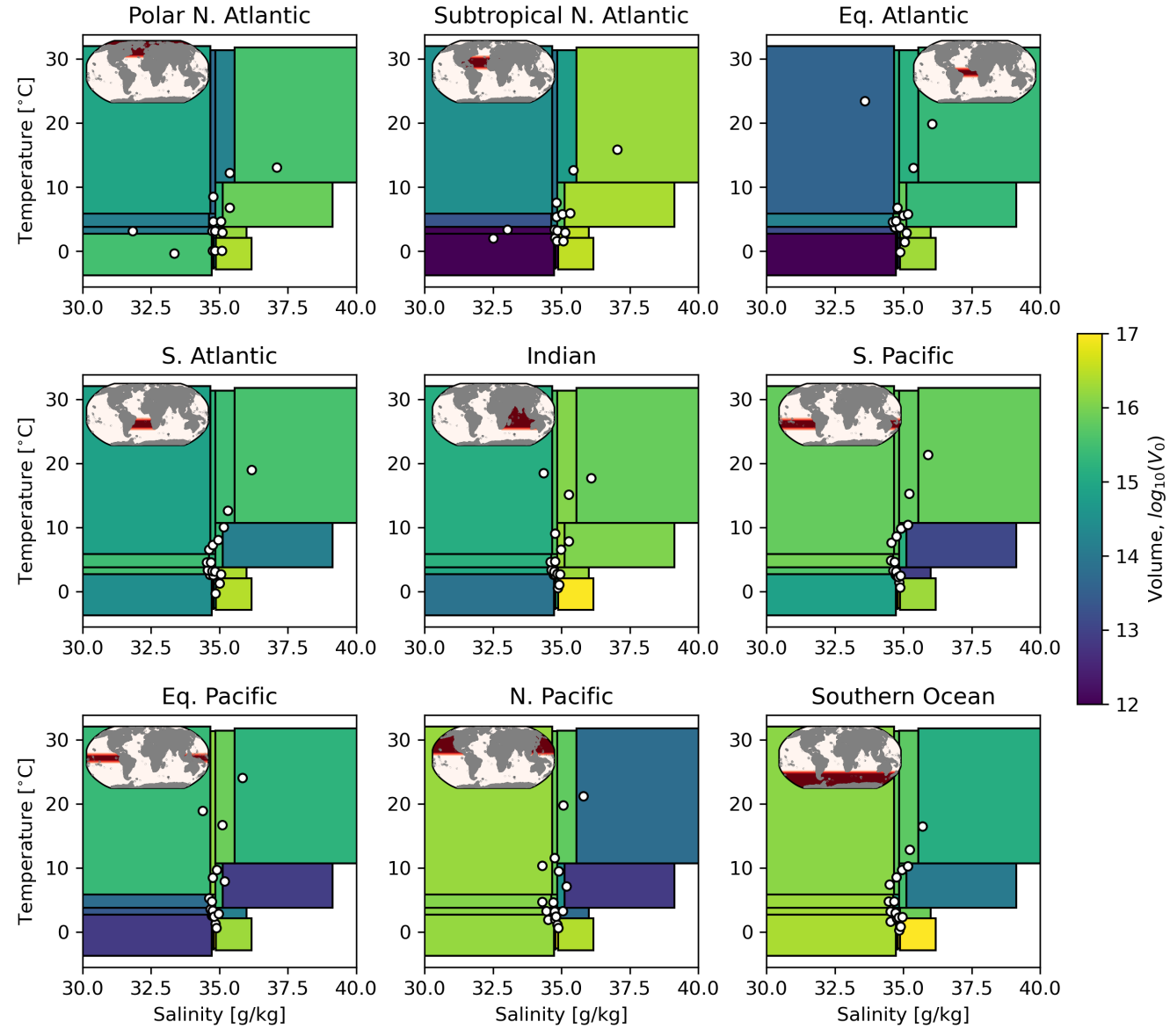

Figure 1. Demonstration of the coarsening achieved through Binary Space Partitioning of the EN4 data set. Each coloured box represents a water mass in T-S space with time-mean T and S bounds as shown by the edges of the boxes. The colour of the box shows the volume held in each water mass. Inset maps show the geographic distribution of the basin that the T-S distribution describes. White dots represent the volume-averaged T and S in each water mass.

the time-mean volume distribution over a given 6 year time window to the time-mean volume distribution over the next 6 year time window. For the COREv2 reanalysis, we use 7 year windows from 1979-1986 to 2000-2006 and obtain three sets

https://doi.org/10.5194/essd-2024-545
Preprint. Discussion started: 13 January 2025

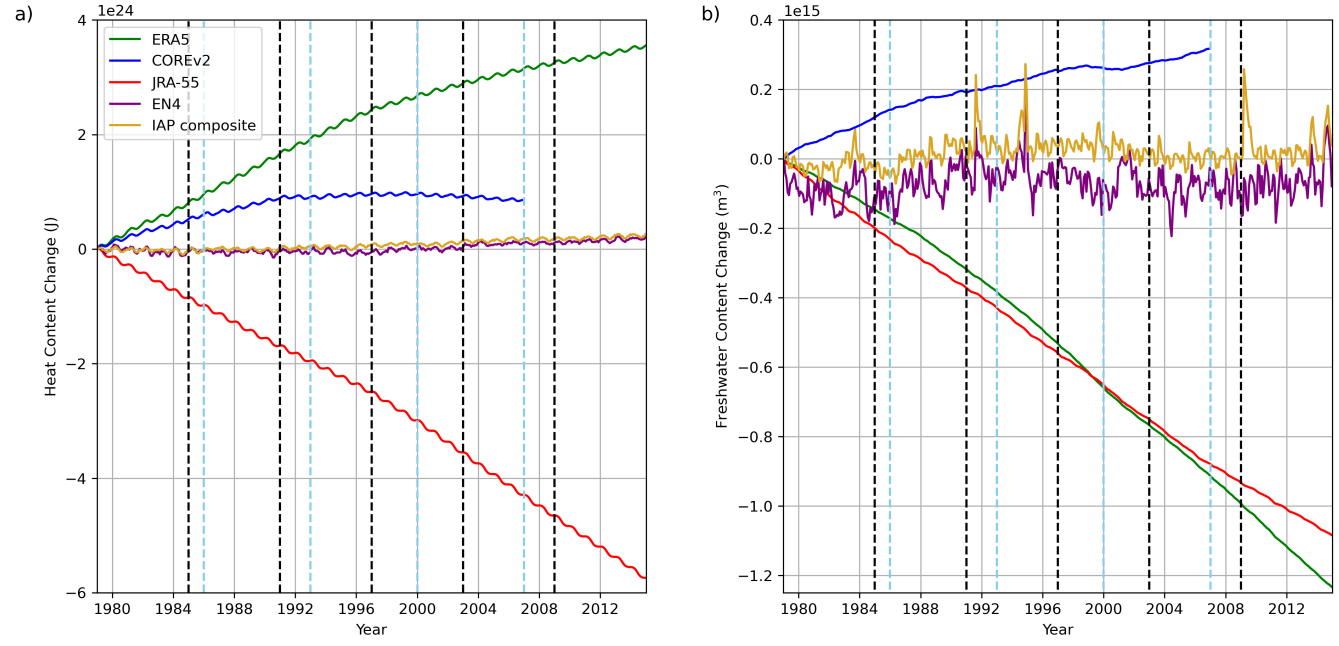

Figure 2. Cumulative a) heat content change and b) freshwater content change implied by air-sea flux products ERA5 (green), JRA-55 (red), and COREv2 (blue), from January 1979 to December 2014 (January 1979 to December 2006 for COREv2), and ocean observations EN4 (purple) and IAP composite data (golden). Dashed vertical lines delineate the time windows over which this analysis is conducted for ERA5 and JRA-55 (black) and COREv2 (light blue).

of g_{ij} transports from OTM. We opt to keep the time windows over which the analysis is conducted shorter than fifteen years, following guidance in Cheng et al. (2022). Figure 2 shows the time windows used in this analysis, with dashed vertical black lines representing the time windows for ERA5 and JRA-55, and dashed vertical light blue lines representing the time windows for COREv2. Applying OTM to these gridded ocean observations and air-sea flux products, we obtain a series of 'adjustments' needed to modify the air-sea heat and freshwater fluxes, such that they are consistent with the volumetric changes in the observations.

Validation of the meridional heat and freshwater transport from OTM also requires comparisons with equivalent transport in climate models and mooring observations. To enable this, we use the pre-industrial control and historical simulations in a suite of climate models which form part of the 6th Climate Model Intercomparison Project (CMIP6). We assess the monthly-averaged meridional heat transport variable (*hfbasin*) in an ensemble of 44 simulations across 21 models to determine the meridional heat transport in the historical simulations, from January 1979 to December 2014 inclusive. The historical meridional heat transport is de-drifted by subtracting the cubic fit over the entire corresponding pre-industrial control time series, following Irving et al. (2020). The CMIP6 data not only provides a constraint on meridional heat transport from coupled climate models, but the inter-model variability also provides an envelope of 'feasible' meridional heat transports.

https://doi.org/10.5194/essd-2024-545
Preprint. Discussion started: 13 January 2025

We also compare our results to the Atlantic Rapid Climate Change-Meridional Overturning Circulation and Heatflux (RAPID-MOCHA, hereafter RAPID) mooring array, a long-term observational network which has been monitoring the strength of the Atlantic Meridional Overturning Circulation (AMOC) at 26.5°N since 2004. We use annual-averaged meridional heat and freshwater transport estimates from RAPID (freshwater transports obtained from McDonagh et al. (2015)), from 2004 to 2014 inclusive, to produce estimates of the heat and freshwater transport at 26.5°N in the North Atlantic, as shown in figure 9c and d and figure 10c and d. In addition, we compare our outputs to annual-averaged heat transport between 2014 and 2018 from the Overturning in the Subpolar North Atlantic Program (OSNAP) array, which lies between 53°N and 60°N. The uncertainty in the time-mean transport in OSNAP and RAPID is taken as the standard deviation of the annual-mean time series (whiskers in figures 9c and 10c). To obtain transport tendencies from OSNAP and RAPID, we take the linear trend in transport over the entire time series. The uncertainty in the tendency (whiskers in figures 9d and 10d) is the standard error of the linear fit, defined as the square-root of the first term in the diagonal of the covariance matrix of the fit.

4 Results

We apply OTM to a combination of three atmosphere/ocean reanalysis products (ERA5, JRA-55 and COREv2), and two gridded hydrographic ocean observational datasets (EN4 and an IAP Composite product).

4.1 Air-sea flux priors and ocean changes

On average, air-sea heat fluxes in JRA-55 suggest significantly more cooling than in COREv2 and ERA5 (compare figure 3b with 3a and c). This trend has been highlighted in past literature and corrected for in the JRA-55 Driving of the Ocean product (JRA-55do; see, for example, Valdivieso et al. (2017); Tsujino et al. (2018)). However, JRA-55do is designed as an input to the bulk formula of Ocean-Sea-Ice models and does not contain the full set of air-sea fluxes required for OTM. The rate of change of air-sea heat fluxes is more consistent across the three reanalysis products (figure 3 d-f), with all three products showing a deceleration of surface warming over the majority of the ocean surface except high latitudes. These trends contrast with the vertically-integrated ocean heat content change from the hydrographic datasets, which broadly suggest an acceleration of ocean warming since 1979 (figure 3g and h).

Overall, the time-mean surface freshwater flux fields show a pattern of precipitation in the tropics, subpolar and polar regions and evaporation in the sub-tropics (see figure 4a - c). The JRA-55 freshwater fluxes are more intensified than ERA5 or COREv2 on average, a pattern identified in past literature that has been rectified in the JRA-55do product (Kobayashi et al., 2015; Tsujino et al., 2018). While the pattern of freshwater flux tendencies is consistent across products, the magnitude of the change is larger in JRA-55 (figure 4d - f). The vertically-integrated ocean freshwater content change from the hydrographic datasets does not align with these freshwater flux tendencies. For instance, the strong increase in precipitation in the tropics does not translate to a corresponding strong freshwater convergence in the gridded observations (compare figure 4d - f and 4g - h).

Observations of ocean heat and salt content suffer from uncertainties, particularly prior to the Argo period in the mid-2000s, and may be contributing to the mismatch between the reanalysis products and ocean observations (Abraham et al., 2013;

https://doi.org/10.5194/essd-2024-545
Preprint. Discussion started: 13 January 2025

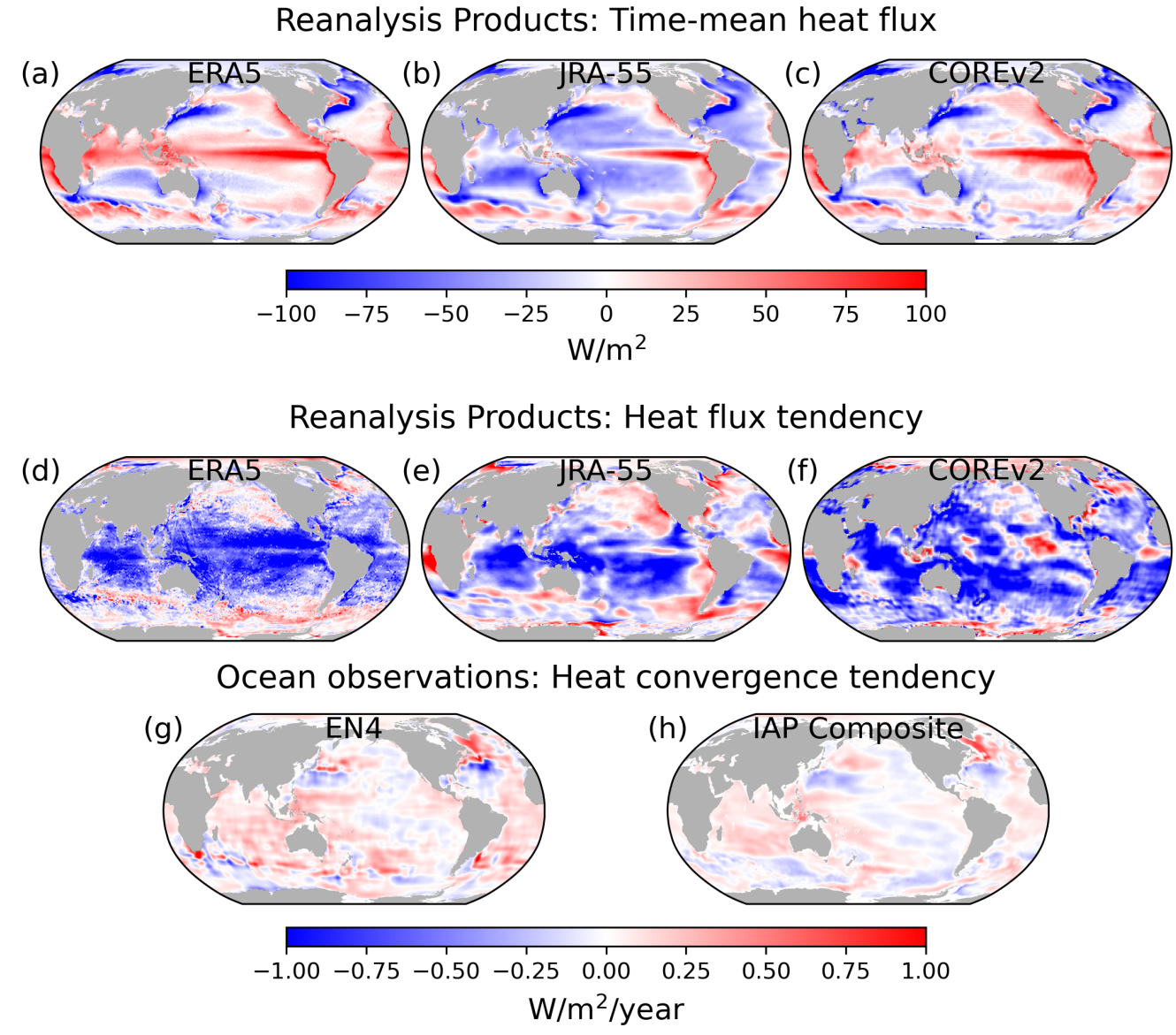

Figure 3. Time-mean surface heat flux fields in a) ERA5, b) JRA-55, and c) COREv2, from January 1979 to December 2014 (January 1979 to December 2006 for COREv2), inclusive, and the heat flux tendency in d) ERA5, e) JRA-55, and f) COREv2 over the same period. Vertically-integrated ocean heat content tendency in the g) EN4 and h) IAP composite gridded hydrographic data sets.

Trenberth et al., 2019). Nevertheless, these maps imply that some adjustment needs to be made to accurately reflect trends in the ocean heat and freshwater budget.

https://doi.org/10.5194/essd-2024-545
Preprint. Discussion started: 13 January 2025

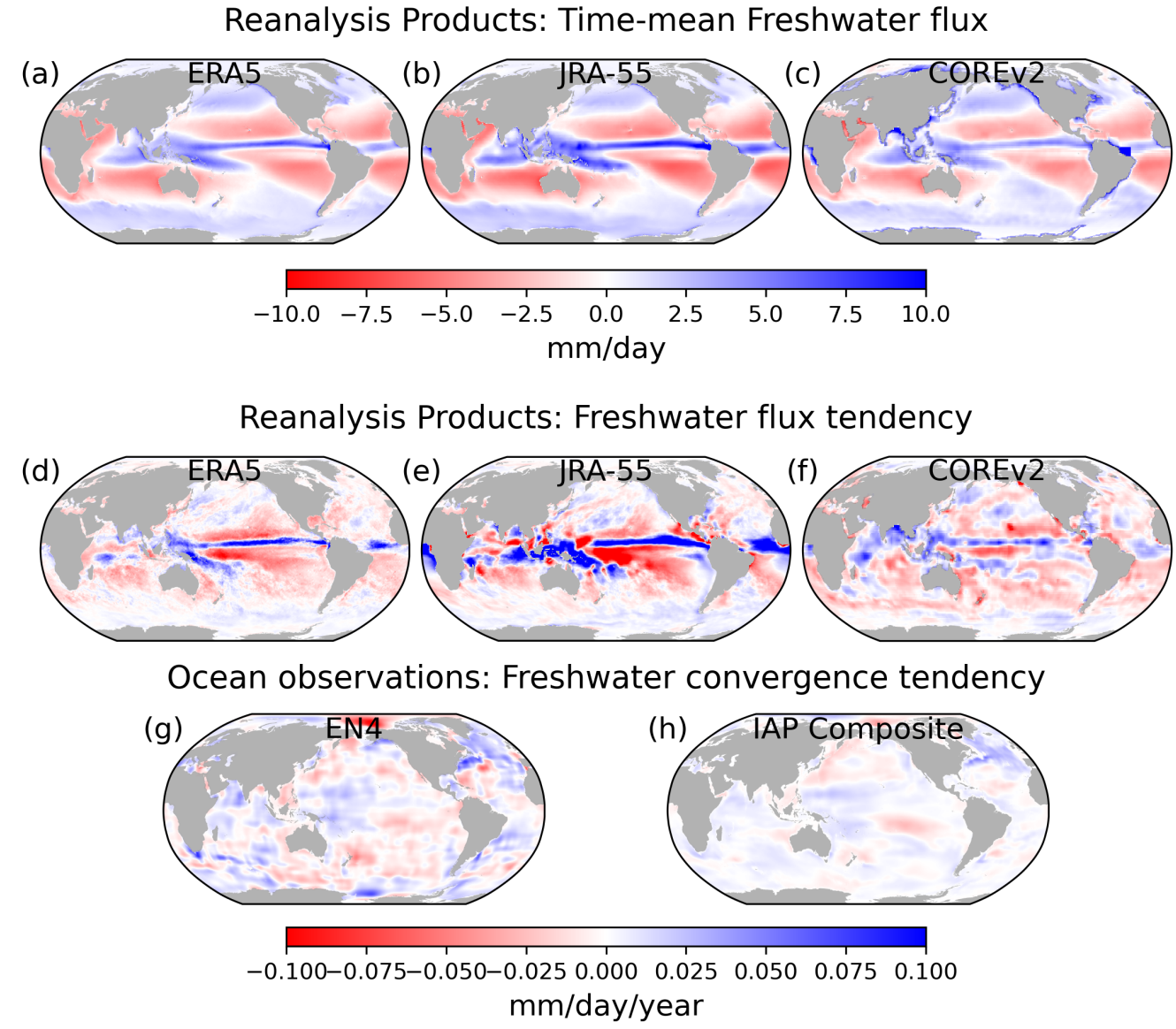

Figure 4. Time-mean surface freshwater flux fields in a) ERA5, b) JRA-55, and c) COREv2, from January 1979 to December 2014 (January 1979 to December 2006 for COREv2), inclusive, and the freshwater flux tendency in d) ERA5, e) JRA-55, and f) COREv2 over the same period. Vertically-integrated ocean freshwater content tendency in the g) EN4 and h) IAP composite gridded hydrographic data sets.

4.2 Adjusted air-sea fluxes

Using OTM, we obtain an estimate of the adjustment to air-sea heat and freshwater fluxes necessary to close the global ocean heat and freshwater budget for each reanalysis product and ocean observation pair (6 adjustments in total). Figure 5 shows

https://doi.org/10.5194/essd-2024-545
Preprint. Discussion started: 13 January 2025

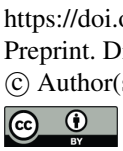

the OTM-based surface heat flux adjustment for the three reanalysis products combined with EN4 (the corresponding plots for the IAP Composite data are shown in figure S2 in the Supplementary Information). Overall, the heat flux adjustment is concentrated in the Southern Ocean and subtropical gyres, with some differences between the Pacific and Atlantic Oceans. The OTM inverse method suggests that warming in the Southern Ocean is too high (or cooling too weak), as the method produces a consistent negative adjustment in this region across all products. Our method also indicates that warming over much of the Pacific is too high in ERA5 (or cooling too small), with the adjustment in this region being consistently negative (see figure 5b). JRA-55, on the other hand, shows too much cooling over much of the globe, and OTM adjusts for this cooling, particularly in the subtropical gyres, with a consistent positive adjustment, as shown in figure 5e. The COREv2 reanalysis product has air-sea heat fluxes that are closest to the observed ocean heat content changes in EN4, thus, the adjustment to COREv2 air-sea heat fluxes is relatively small (figure 5h).

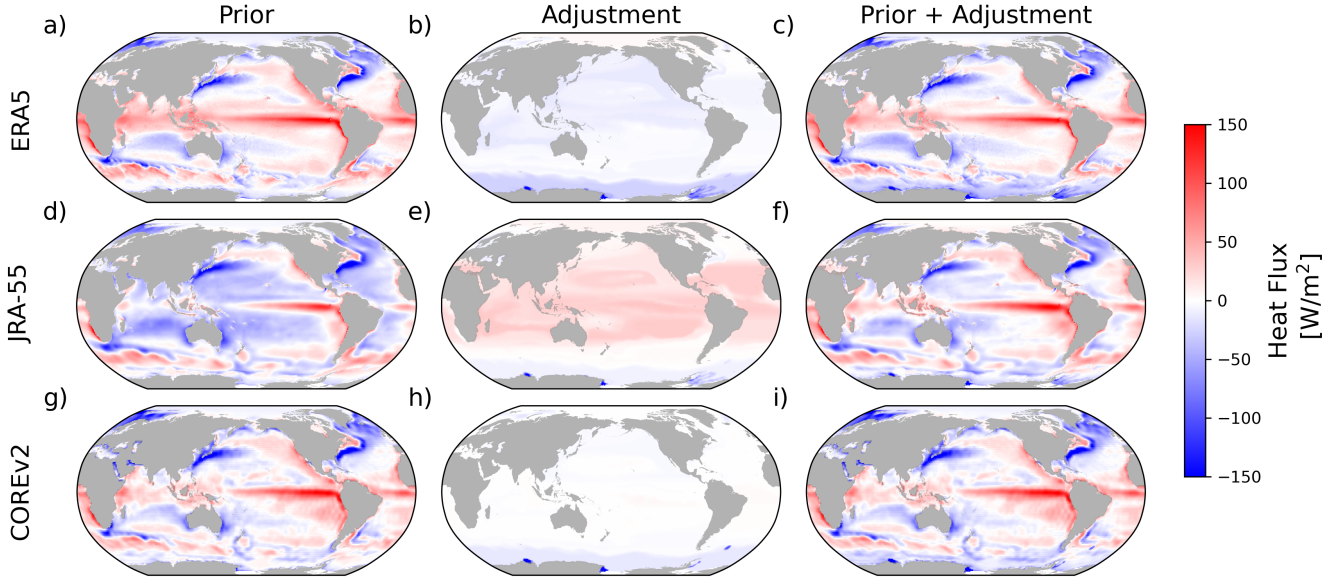

Figure 5. Time-mean surface heat fluxes and adjustments of reanalysis products when combined with EN4 gridded data. a), d) and g) Time-mean prior surface air-sea heat fluxes in ERA5, JRA-55 and COREv2, respectively. b), e) and h) The inferred adjustment necessary to reconcile surface heat fluxes with the EN4-based ocean heat content tendency from OTM in ERA5, JRA-55 and COREv2, respectively. c), f) and i) the sum of the surface heat flux priors and the necessary adjustments in ERA5, JRA-55 and COREv2, respectively.

Note that the adjustment obtained from OTM is influenced by the weight we impose on the cost function. In this case, we choose to weight the optimal transformation function by the inter-product difference in air-sea heat and freshwater fluxes. The Southern Ocean has a particularly large difference in air-sea heat fluxes between reanalysis products, so our model imposes a lower penalty to adjusting the air-sea heat fluxes in this region. Thus, the consistently negative heat flux adjustment in the Southern Ocean and Antarctic margins shown in figure 5 may be a consequence of our method, rather than a 'true' error in this region.

https://doi.org/10.5194/essd-2024-545
Preprint. Discussion started: 13 January 2025

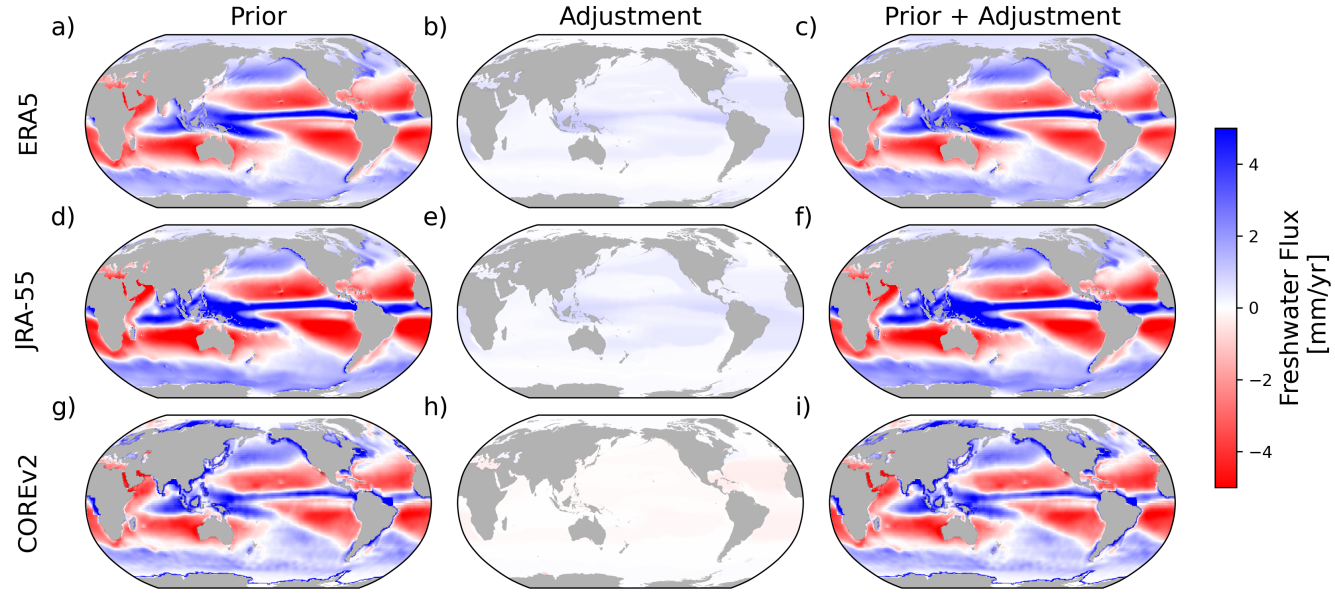

Figure 6. Time-mean surface freshwater fluxes and adjustments of reanalysis products when combined with EN4 gridded data. a), d) and g) Time-mean prior surface air-sea freshwater fluxes in ERA5, JRA-55 and COREv2, respectively. b), e) and h) The inferred adjustment necessary to reconcile surface freshwater fluxes with the EN4-based ocean freshwater content tendency from OTM in ERA5, JRA-55 and COREv2, respectively. c), f) and i) the sum of the surface freshwater flux priors and the necessary adjustments in ERA5, JRA-55 and COREv2, respectively.

As with surface heat fluxes, OTM provides a physically-constrained adjustment to freshwater fluxes in the reanalysis products so they align with observed salinity changes. The OTM-based adjustment of freshwater fluxes is shown in figure 6 for EN4 (the corresponding plots for the IAP composite data are shown in figure S2 in the Supplementary Information). In ERA5 and JRA-55, the adjustment obtained from OTM shows an increased net precipitation in the tropics and subtropics. This enhanced net precipitation is particularly concentrated around the Indo-Pacific tropics and Atlantic subtropical gyres (see figure 6b and e). The net effect of such an adjustment is an enhancement of tropical Indo-Pacific precipitation in these reanalysis products and a reduction of evaporation in the Atlantic basin (as in figure 6c and f). In COREv2, on the other hand, the OTM-based adjustment shows a slightly enhanced net evaporation globally, particularly in the Atlantic subtropical gyres. As with surface heat fluxes, the COREv2 adjustment is relatively small compared with ERA5 and JRA-55.

The net effect of these air-sea flux adjustments is explored by zonally-integrating the air-sea flux fields across all combinations of reanalysis products and ocean observations, in figure 7. While the adjustment modifies the COREv2 air-sea heat fluxes very little (figure 7e), the JRA-55 and ERA5 heat fluxes are quasi-uniformly adjusted in opposite directions such that the adjusted fields have a similar pattern, with net cooling in the subtropics (at $\pm 40^\circ$ latitudes) and warming equatorward of $\pm 20^\circ$ (see figure 7a and c). Thus, OTM adjusts heat flux patterns so they look similar across the 6 combinations of data products explored. The net impact of freshwater flux adjustments, on the other hand, is relatively small, with broad net precipitative

https://doi.org/10.5194/essd-2024-545
Preprint. Discussion started: 13 January 2025

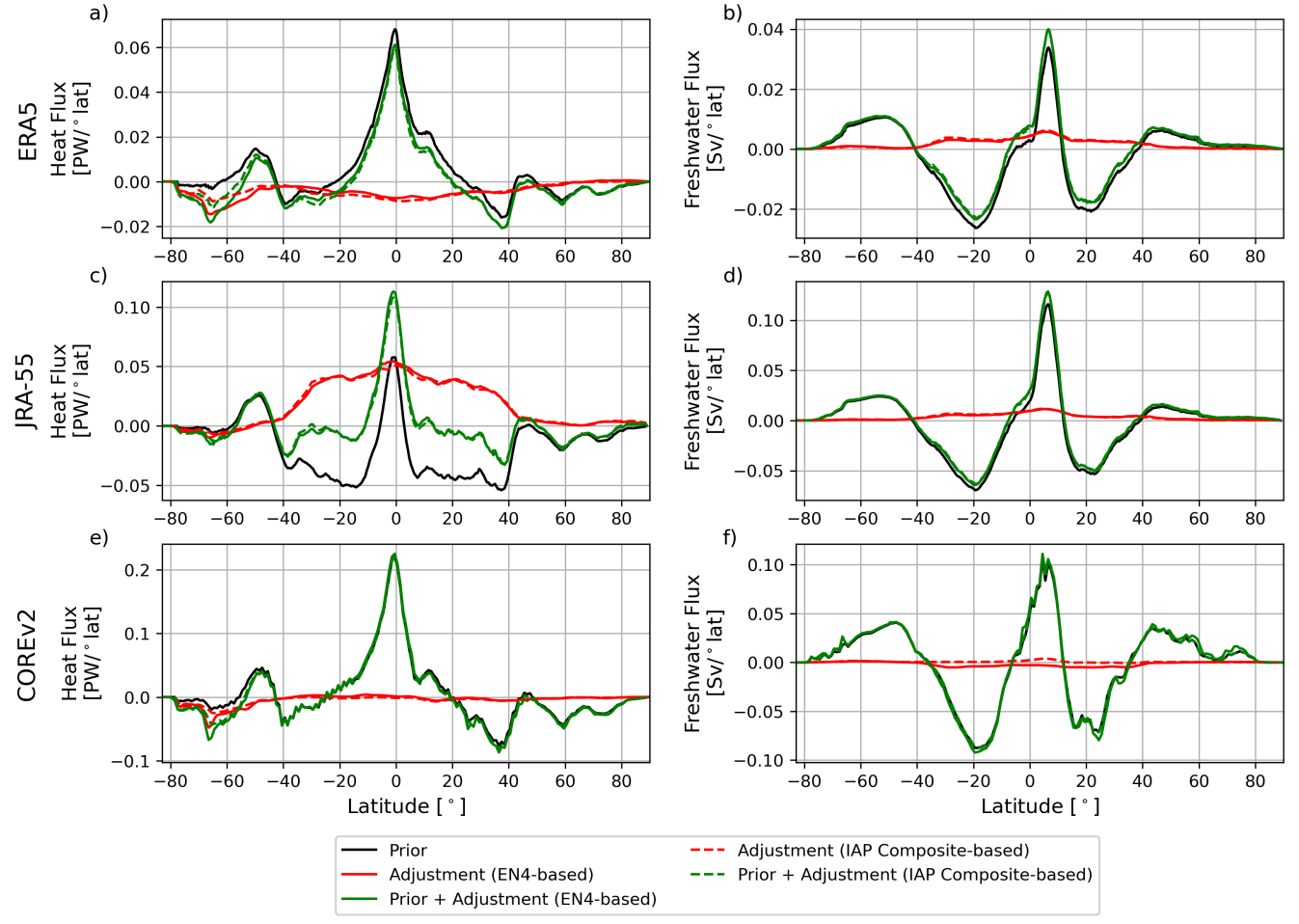

Figure 7. Zonally-integrated surface heat and freshwater flux priors (black), inferred EN4-based adjustment (red) and sum of the two (green). Solid lines show the adjustment when combined with EN4 data, and dashed lines show the adjustment for IAP composite data.

adjustments in ERA5 and JRA-55, and a smaller net evaporative adjustment in COREv2. There results demonstrate that OTM can flexibly adjust heat and freshwater fluxes asymmetrically, as the ERA5 adjustment cools and freshens globally, while the JRA-55 adjustment warms and freshens globally.

The impact of the OTM-based adjustment on global heat and freshwater is investigated further by interrogating the mean heat and freshwater budget terms integrated over ocean basins, as in figure 8. The budget terms are the ocean tracer content (dOTC, red bars), the prior surface air-sea fluxes (Q_{prior}, green bars), the tracer transport divergence (i.e., inter-basin heat or freshwater transport; gold bars) and the air-sea flux adjustment. In order to compare OTM with other means of reconciling air-sea heat flux biases with tracer observations, we compare the OTM-based adjustment ($Q_{adj,OTM}$, purple bars) with an adjustment that uniformly redistributes the global air-sea flux bias ($Q_{adj,uniform}$, black outline bars) and an adjustment that

https://doi.org/10.5194/essd-2024-545
Preprint. Discussion started: 13 January 2025

Open Access Earth System Science Data Discussions

redistributes the global air-sea flux bias scaled by the root-mean-squared-error across all reanalysis products ($Q_{adj,RMSE}$, blue outline bars). There is significant inter-basin and inter-product variance in the heat budget terms in figure 8a - c. For example, the Q_{prior} in the Equatorial Pacific varies in sign between ERA5 and JRA-55. As a result, the adjustment term varies between the two products, resulting in a similar magnitude transport divergences. The largest differences between the different methods of heat flux adjustment occur in the Southern Ocean. Despite relatively small Q_{prior} across all three products in the Southern Ocean, the flux adjustment varies significantly depending on the adjustment method. In ERA5 and COREv2, the OTM-based adjustment in the Southern Ocean is larger than the uniform adjustment, and much larger than the RMSE-based adjustment. In JRA-55, on the other hand, the OTM-based adjustment is opposite sign (and smaller magnitude) than the uniform and RMSE-based adjustment. The substantial differences in heat flux adjustments in the Southern Ocean may be related to the OTM method, which is weighted by the inter-product RMSD, meaning that OTM is particularly permissive of flux adjustments in the highly uncertain Southern Ocean.

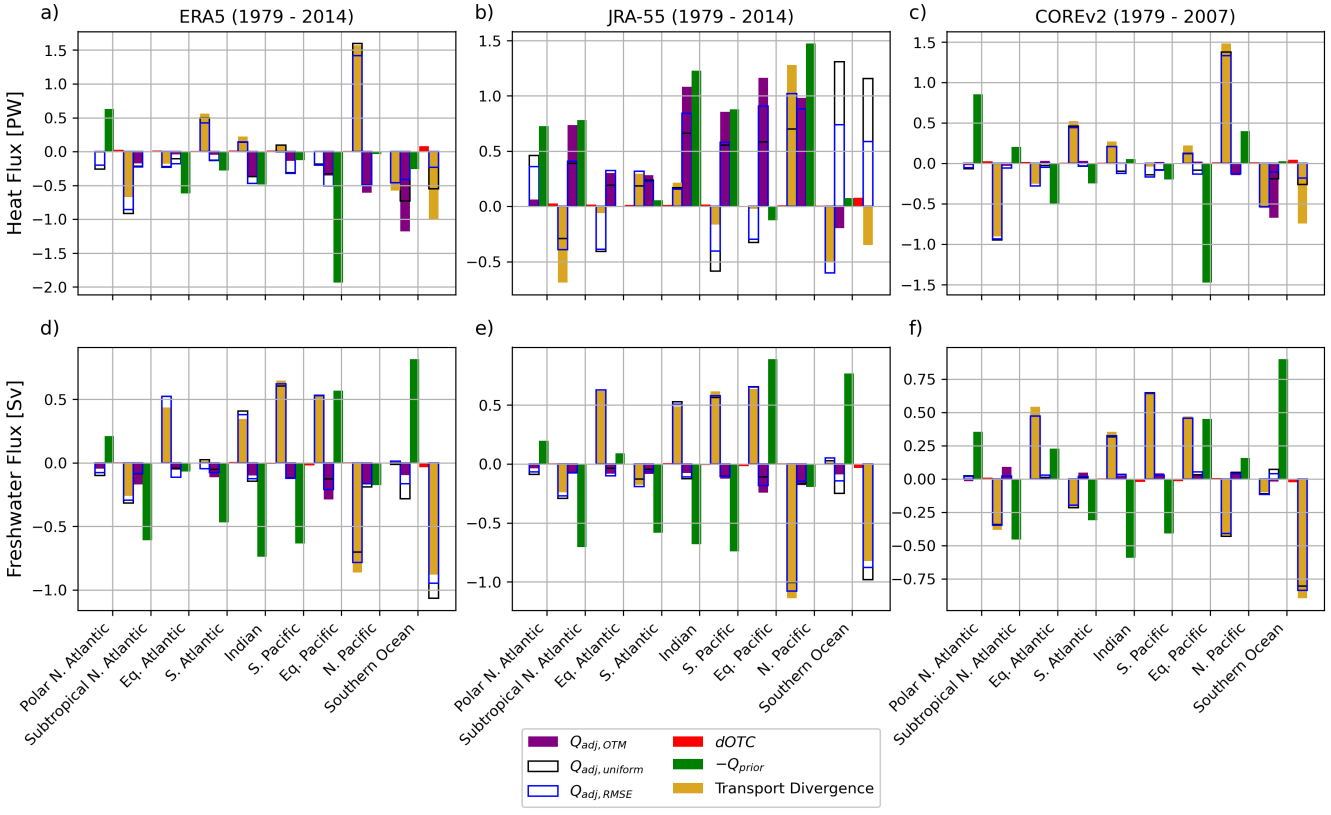

Figure 8. Time-mean basin-scale heat and freshwater budgets for reanalysis products combined with EN4 observations. a) - c) Basin-scale heat budget terms for ERA5, JRA-55 and COREv2, respectively. d) - f) Basin-scale freshwater budget terms for ERA5, JRA-55 and COREv2, respectively. The geographic boundaries of basins is shown in the inset maps in figure 1.

https://doi.org/10.5194/essd-2024-545
Preprint. Discussion started: 13 January 2025

The prior air-sea freshwater fluxes appear to be more similar across the three reanalysis products explored. The largest point of difference here is again in the Southern Ocean. The OTM-based adjustment is negative for all reanalysis products in the Southern Ocean, but varies significantly from the other adjustment methods explored. In ERA5 and JRA-55, the OTM-based adjustment is a similar order of magnitude to the RMSE-based adjustment. In COREv2, the RMSE-based and uniform adjustments are of opposite sign to the OTM-based freshwater flux adjustment. That said, the freshwater flux adjustments are relatively small, so the freshwater transport divergence is similar across the reanalysis products and adjustment methods explored here.

4.3 Meridional heat and freshwater transport

The adjusted time-mean adjusted surface air-sea flux fields also enable the analysis of meridional heat and freshwater transports. We diagnose meridional heat transport as the residual between air-sea heat fluxes (adjusted using OTM, as shown in figure 5c, f and i) and vertically-integrated ocean heat content change, following Trenberth and Fasullo (2017). The longitudinally-integrated meridional heat transport is shown in figure 9 for all combinations of reanalysis products and gridded observations, globally and in the Atlantic and Indo-Pacific. Overall, the time-mean meridional heat transport shows the global poleward redistribution of heat as part of the planetary 'heat engine'. Averaged across all products, the maximal global poleward heat transport is 1.6 PW at 17°N, and 0.8 PW at 16°S (figure 9a). Much of the northward heat transport comes from the Atlantic basin, which has a maximum northward heat transport of 1 PW at 23°N (figure 9c). The Indo-Pacific also hosts poleward heat transports of 0.6 PW at 17°N and 1.2 PW at 13°S.

The time-mean ocean heat transports inferred from OTM match closely with prior research using the ECCO state estimate (Forget and Ferreira, 2019) and climate models (Mecking and Drijfhout, 2023), and have relatively small differences across products. We further compare our observational meridional ocean heat transport trends with climate model historical simulations (from CMIP6). In the 21 models analysed (consisting of a total of 44 realisations of the historical simulation), we see a similar multi-model mean absolute value for meridional heat transport as obtained from OTM (black line in figure 9a).

The meridional heat transport tendency generally shows a slowdown in global poleward heat transport, but with significant variance in magnitude and location depending on the combination of products used (figure 9b). This long-term slowdown in poleward heat transport has been seen in ocean and climate models (e.g., Armour et al. (2016); Huguenin et al. (2022); Mecking and Drijfhout (2023)), but has not previously been quantified in long-term ocean observations. However, the global tendency estimates here are different depending on the product and the choice of parameters in the OTM algorithm - in particular, the weights placed on the cost function. In addition, while the CMIP6 meridional heat transport tendency does indicate a slowdown in poleward heat transport, it is by significantly less than our estimates (see figure 9b). This indicates that further constraints need to be added to OTM to ensure it adequately adjusts long-term heat flux tendencies. Note that in the present version of OTM, all that is required is that the transformations of the ocean's water masses over time do not break basic thermodynamic laws. No constraints have been placed on the dynamics of the ocean.

While no direct long-term observations of heat transport exist from 1979 to 2014, direct observations *are* available from the RAPID and OSNAP mooring arrays in the Atlantic, which have been continuously recording the strength of the ocean

https://doi.org/10.5194/essd-2024-545
Preprint. Discussion started: 13 January 2025

circulation and meridional heat transport since 2004 (for RAPID) and 2014 (for OSNAP) (Moat et al., 2022; Fu et al., 2023a). RAPID is located at 26.5°N in the Atlantic Ocean, providing a single direct observational constraint to compare with our results. OSNAP covers a range of latitudes, between 53°N and 60°N, and we show the OSNAP measurements at 59°N as an average. The time-mean meridional heat transport from RAPID (averaged between 2004 and 2014 and shown in figure 9c in black) agrees with the inferred estimates from ERA5 and COREv2 in this study. The meridional heat transport in OSNAP has a narrower range of possible time-mean meridional heat transports (averaged between 2014 and 2018 and shown in figure 9c in purple), and lies between OTM-based inferred heat transports from ERA5 and COREv2 in the Atlantic. However, in the Atlantic, and particularly in the Indo-Pacific, there is a lack of agreement between reanalysis products on the meridional heat transport tendency (figures 9d and f). Nevertheless, the comparison with RAPID and OSNAP provides some confidence that our inverse method may be accurately representing the time-mean ocean heat transport. Note that the basin-scale meridional transports are only interpretable north of 35°S (outside hatched area in figure 9c - f). South of this latitude, the Antarctic Circumpolar Current (ACC) contributes large horizontal tracer divergences, which impact the basin-scale (but not global) meridional transports.

We also assess the meridional freshwater transport as the residual of adjusted air-sea freshwater fluxes and ocean freshwater content change (figure 10). The time-mean global freshwater transport in figure 10a reflects the redistribution of freshwater from the (relatively fresh) poles and tropics to the (relatively salty) sub-tropics. The maximum freshwater divergence in the sub-polar regions is 0.64 Sv at 37°N, and the maximal freshwater convergence in the Northern hemisphere subtropics is 0.53 Sv at 13 °N. There is also a substantial freshwater divergence out of the tropics, which peaks at 0.83 Sv at 6°S. In the Southern hemisphere, there is broad freshwater convergence, which is largest at 0.95 Sv at 40°S.

The freshwater transport tendency (figure 10b) varies substantially between reanalysis products in the Northern Hemisphere, but shows a more consistent reduction in freshwater transport in the Southern Hemisphere. While we do not have access to direct global observations which can verify such a trend, our heat transport tendency results suggest there may be a low confidence in these findings. Thus, further development of the OTM setup is necessary to better constrain these freshwater tendencies. Note, as with heat transports, we do not interpret the freshwater transports below 35°S (the hatched area in figure 10c - f) as they are influenced by the ACC.

A significant portion of the global freshwater transport out of the polar and sub-polar regions comes from the Atlantic in the Northern Hemisphere (see inferred transport north of 20°N in figure 10c). The Atlantic freshwater divergence peaks at 0.27 Sv at 42°N and freshwater convergence is highest at 0.27 Sv at 12°N. In addition, the Indo-Pacific is the largest contributor to global freshwater transport out of the tropics (see inferred transport between 20°N and 20°S in figure 10e). The Indo-Pacific freshwater divergence out of the sub-polar regions is highest at 0.4 Sv at 34°N, and out of the tropics peaks at 0.92 Sv at 9°S. The Indo-Pacific contribution to freshwater convergence into the sub-tropics is maximal at 0.25 Sv at 13°N.

The freshwater transport tendencies in the Atlantic and Indo-Pacific differ depending on the choice of reanalysis and observational product. Our main point of comparison with these freshwater transports is a direct measurement from the RAPID program at 26.5°N in the Atlantic Ocean. The RAPID time-mean freshwater transport and transport tendencies both fall outside our OTM-based inferred freshwater transport estimates in the Atlantic (see black dots and whiskers in figure 10c and d).

https://doi.org/10.5194/essd-2024-545
Preprint. Discussion started: 13 January 2025

However, the time-mean inferred transports are closer to the RAPID estimates than the tendencies. In the future, direct constraints could be implemented within the OTM framework to align the inferred freshwater transports with direct observations in the Atlantic.

5 Discussion

The OTM framework presents a computationally efficient, flexible means of reconciling biased air-sea flux products with observed tracer changes in the global ocean. Using OTM, we present a set of 'adjusted' ERA5, JRA-55 and COREv2 reanalysis flux fields that match global ocean trends from observations. Using OTM to adjust reanalysis flux fields presents an alternative to 'traditional' means of reconciling global heat and freshwater budgets, which redistribute air-sea flux biases uniformly, or based on the inter-product RMSE. While the inter-product variance of the time-mean OTM-adjusted air-sea fluxes is relatively small (i.e., the adjusted fields are similar), the trends in the adjusted air-sea flux fields vary significantly between products. In addition, the magnitude of the time-mean air-sea freshwater fluxes may not be adequately adjusted by OTM (compare JRA-55 adjusted freshwater flux fields to ERA5 and COREv2 in figure 6). This is because the OTM algorithm is relatively unconstrained - we do not impose transport or flux constraints, and our choice of weighting of the cost function can alter the outputs. OTM can thus account for amplified patterns with a larger transport between regions (larger in JRA-55 than in ERA5 and COREv2, in this case). This transport must also distribute heat along with fresh water. In fact, the adjustment of JRA-55 towards more low latitude warming and high latitude cooling is consistent with a solution with amplified meridional transport.

Future development of the OTM framework could introduce additional transport constraints (through the Bering Strait, for instance, as in Mackay et al. (2024)), additional tracers (also as in Mackay et al. (2024)) or more complex weighting of the cost function, to refine long-term trends. In addition, a larger range of reanalysis products and ocean observational products could be used to better understand the uncertainty in our analysis. Despite these areas of improvement, the OTM algorithm does enable us to develop adjusted time-mean air-sea flux fields that may be used for global heat and freshwater analyses in the future. The adjusted time-mean air-sea flux fields and the heat and freshwater transports inferred from OTM are publicly shared as part of this analysis.

6 Conclusions

In this work, we have combined air-sea heat flux products with ocean observations to diagnose long-term heat and freshwater fluxes, as well as meridional transport, purely from observations. Using a novel inverse method, termed the 'Optimal Transformation Method' (OTM), we leverage the unique properties of mixing and circulation to adjust atmospheric reanalysis products such that they align with ocean observations. Thus, we obtain 'adjusted' air-sea heat and freshwater fluxes since 1979 that have a closed global heat and freshwater budget (derived from ERA5, COREv2 and JRA-55). Our results for the time-mean state of the system are relatively consistent when different data sources are used. However, our implementation of the optimal transformation method, which constrains air-sea fluxes to obey basic laws of tracer conservation and mixing, does not dramatically

https://doi.org/10.5194/essd-2024-545
Preprint. Discussion started: 13 January 2025

narrow the broad range of possible trends estimated by atmospheric reanalyses. We have made the time-mean adjusted air-sea flux fields and the implied meridional heat and freshwater transports openly available for future research on Zenodo (Sohail and Zika, 2024, doi: 10.5281/zenodo.14004937).

7 Code and data availability

All reanalysis and data products used in this study are publicly available. ERA5 reanalysis data can be obtained from the European Centre for Medium-Range Weather Forecasts, ECMWF (Hersbach et al., 2023, doi: 10.24381/cds.6860a573), JRA-55 reanalysis data is available from the Japan Meteorological Agency, JMA (http://search.diasjp.net/en/dataset/JRA55), and COREv2 reanalysis data is provided by National Center for Atmospheric Research, NCAR (Yeager and Large, 2008, doi: 10.5065/D6WH2N0S). Ocean gridded datasets from are available from the UK Met Office Hadley Center (EN4 data: https://www.metoffice.gov.uk/hadobs/en4/) and the Institute of Atmospheric Physics, Chinese Academy of Sciences (IAP data: http://www.ocean.iap.ac.cn/pages/dataService/dataService.html).

Meridional heat and freshwater transports are obtained from the RAPID-MOCHA and OSNAP arrays (RAPID-MOCHA data at (Johns et al., 2023, doi: 10.17604/3nfq-va20) ; OSNAP data at (Fu et al., 2023b, doi: 10.35090/gatech/70342)). A minimal working example of the OTM algorithm, using model validation data, is provided at Zenodo (Zika and Sohail, 2024, doi: 10.5281/zenodo.8008629), and further information on the algorithm is given in Zika and Sohail (2023). The adjusted surface reanalysis fields obtained in this analysis, and the inferred meridional heat and freshwater transports are provided at Zenodo (Sohail and Zika, 2024, doi: 10.5281/zenodo.14004937).

Author contributions. JDZ conceived the Optimal Transformation Method, and further development occurred between JDZ and TS over several years. TS developed the working code base based on an initial proof-of-concept code written by JDZ. All calculations, visualisations and analysis were conducted by TS, with substantial input from JDZ. TS wrote the text, with contributions from JDZ.

Competing interests. The authors declare no competing interests.

Acknowledgements. The authors acknowledge support from the Australian Center for Excellence in Antarctic Science (ACEAS; grant no. SR200100008) and the Australian Research Council Discovery Projects (grant no. DP190101173). The authors also acknowledge ECMWF, JMA, NCAR, the UK Met Office, Lijing Cheng, and the RAPID-MOCHA and OSNAP projects for furnishing the relevant data sets that enabled this analysis. The authors thank Dr. Neill Mackay for their helpful feedback during the development of the OTM algorithm.

https://doi.org/10.5194/essd-2024-545
Preprint. Discussion started: 13 January 2025

References

Abraham, J. P., Baringer, M., Bindoff, N. L., Boyer, T., Cheng, L. J., Church, J. A., Conroy, J. L., Domingues, C. M., Fasullo, J. T., Gilson, J., Goni, G., Good, S. A., Gorman, J. M., Gouretski, V., Ishii, M., Johnson, G. C., Kizu, S., Lyman, J. M., Macdonald, A. M., Minkowycz, W. J., Moffitt, S. E., Palmer, M. D., Piola, A. R., Reseghetti, F., Schuckmann, K., Trenberth, K. E., Velicogna, I., and Willis, J. K.: A review of global ocean temperature observations: Implications for ocean heat content estimates and climate change, Reviews of Geophysics, 51, 450–483, https://doi.org/10.1002/rog.20022, 2013.

Armour, K. C., Marshall, J., Scott, J. R., Donohoe, A., and Newsom, E. R.: Southern Ocean warming delayed by circumpolar upwelling and equatorward transport, Nature Geoscience, 9, 549–554, https://doi.org/10.1038/ngeo2731, 2016.

Arumí-Planas, C., Dong, S., Perez, R., Harrison, M. J., Farneti, R., and Hernández-Guerra, A.: A Multi-Data Set Analysis of the Freshwater Transport by the Atlantic Meridional Overturning Circulation at Nominally 34.5°S, Journal of Geophysical Research: Oceans, 129, https://doi.org/10.1029/2023jc020558, 2024.

Balmaseda, M., Hernandez, F., Storto, A., Palmer, M., Alves, O., Shi, L., Smith, G., Toyoda, T., Valdivieso, M., Barnier, B., Behringer, D., Boyer, T., Chang, Y.-S., Chepurin, G., Ferry, N., Forget, G., Fujii, Y., Good, S., Guinehut, S., Haines, K., Ishikawa, Y., Keeley, S., Köhl, A., Lee, T., Martin, M., Masina, S., Masuda, S., Meyssignac, B., Mogensen, K., Parent, L., Peterson, K., Tang, Y., Yin, Y., Vernieres, G., Wang, X., Waters, J., Wedd, R., Wang, O., Xue, Y., Chevallier, M., Lemieux, J.-F., Dupont, F., Kuragano, T., Kamachi, M., Awaji, T., Caltabiano, A., Wilmer-Becker, K., and Gaillard, F.: The Ocean Reanalyses Intercomparison Project (ORA-IP), Journal of Operational Oceanography, 8, s80–s97, https://doi.org/10.1080/1755876x.2015.1022329, 2015.

Basinski-Ferris, A. and Zanna, L.: Estimating freshwater flux amplification with ocean tracers via linear response theory, Earth System Dynamics, 15, 323–339, https://doi.org/10.5194/esd-15-323-2024, 2023.

Bentamy, A., Piollé, J., Grouazel, A., Danielson, R., Gulev, S., Paul, F., Azelmat, H., Mathieu, P., Schuckmann, K. v., Sathyendranath, S., Evers-King, H., Esau, I., Johannessen, J., Clayson, C., Pinker, R., Grodsky, S., Bourassa, M., Smith, S., Haines, K., Valdivieso, M., Merchant, C., Chapron, B., Anderson, A., Hollmann, R., and Josey, S.: Review and assessment of latent and sensible heat flux accuracy over the global oceans, Remote Sensing of Environment, 201, 196–218, https://doi.org/10.1016/j.rse.2017.08.016, 2017.

Bryan, K.: Poleward Heat Transport by the Ocean: Observations and Models, Annual Review of Earth and Planetary Sciences, 10, 15–38, https://doi.org/10.1146/annurev.ea.10.050182.000311, 1982.

Cheng, L. and Zhu, J.: Benefits of CMIP5 multimodel ensemble in reconstructing historical ocean subsurface temperature variations, Journal of Climate, 29, 5393–5416, https://doi.org/10.1175/jcli-d-15-0730.1, 2016.

Cheng, L., Trenberth, K. E., Gruber, N., Abraham, J. P., Fasullo, J. T., Li, G., Mann, M. E., Zhao, X., and Zhu, J.: Improved estimates of changes in upper ocean salinity and the hydrological cycle, Journal of Climate, 33, 1–74, https://doi.org/10.1175/jcli-d-20-0366.1, 2020.

Cheng, L., Foster, G., Hausfather, Z., Trenberth, K. E., and Abraham, J.: Improved Quantification of the Rate of Ocean Warming, Journal of Climate, 35, 4827–4840, https://doi.org/10.1175/jcli-d-21-0895.1, 2022.

Durack, P. J., Wijffels, S. E., and Matear, R. J.: Ocean Salinities Reveal Strong Global Water Cycle Intensification During 1950 to 2000, Science, 336, 455–458, https://doi.org/10.1126/science.1212222, 2012.

Forget, G. and Ferreira, D.: Global ocean heat transport dominated by heat export from the tropical Pacific, Nature Geoscience, 12, 351–354, https://doi.org/10.1038/s41561-019-0333-7, 2019.

Fu, Y., Lozier, M. S., Biló, T. C., Bower, A. S., Cunningham, S. A., Cyr, F., Jong, M. F. d., deYoung, B., Drysdale, L., Fraser, N., Fried, N., Furey, H. H., Han, G., Handmann, P., Holliday, N. P., Holte, J., Inall, M. E., Johns, W. E., Jones, S., Karstensen, J., Li, F., Pacini, A.,

https://doi.org/10.5194/essd-2024-545
Preprint. Discussion started: 13 January 2025

Pickart, R. S., Rayner, D., Straneo, F., and Yashayaev, I.: Seasonality of the Meridional Overturning Circulation in the subpolar North Atlantic, Communications Earth & Environment, 4, 181, https://doi.org/10.1038/s43247-023-00848-9, 2023a.

Fu, Y., Lozier, M. S., Biló, T. C., Bower, A. S., Cunningham, S. A., Cyr, F., Jong, M. F. d., deYoung, B., Drysdale, L., Fraser, N., Fried, N., Furey, H. H., Han, G., Handmann, P., Holliday, N. P., Holte, J., Inall, M. E., Johns, W. E., Jones, S., Karstensen, J., Li, F., Pacini, A., Pickart, R. S., Rayner, D., Straneo, F., and Yashayaev, I.: Meridional Overturning Circulation Observed by the Overturning in the Subpolar North Atlantic Program (OSNAP) Array from August 2014 to June 2020 [Dataset], https://doi.org/10.35090/gatech/70342, 2023b.

Good, S. A., Martin, M. J., and Rayner, N. A.: EN4: Quality controlled ocean temperature and salinity profiles and monthly objective analyses with uncertainty estimates, Journal of Geophysical Research: Oceans, 118, 6704–6716, https://doi.org/10.1002/2013jc009067, 2013.

Grist, J. P., Josey, S. A., Zika, J. D., Evans, D. G., and Skliris, N.: Assessing recent air-sea freshwater flux changes using a surface temperature-salinity space framework, Journal of Geophysical Research: Oceans, 121, 8787–8806, https://doi.org/10.1002/2016jc012091, grist et al., 2016: Great paper to be cited in future., 2016.

Groeskamp, S., Griffies, S. M., Iudicone, D., Marsh, R., Nurser, A. J. G., and Zika, J. D.: The Water Mass Transformation Framework for Ocean Physics and Biogeochemistry, Annual Review of Marine Science, 11, 271–305, https://doi.org/10.1146/annurev-marine-010318-095421, 2019.

Hersbach, H., Bell, B., Berrisford, P., Hirahara, S., Horányi, A., Muñoz-Sabater, J., Nicolas, J., Peubey, C., Radu, R., Schepers, D., Simmons, A., Soci, C., Abdalla, S., Abellan, X., Balsamo, G., Bechtold, P., Biavati, G., Bidlot, J., Bonavita, M., Chiara, G., Dahlgren, P., Dee, D., Diamantakis, M., Dragani, R., Flemming, J., Forbes, R., Fuentes, M., Geer, A., Haimberger, L., Healy, S., Hogan, R. J., Hólm, E., Janisková, M., Keeley, S., Laloyaux, P., Lopez, P., Lupu, C., Radnoti, G., Rosnay, P., Rozum, I., Vamborg, F., Villaume, S., and Thépaut, J.: The ERA5 global reanalysis, Quarterly Journal of the Royal Meteorological Society, 146, 1999–2049, https://doi.org/10.1002/qj.3803, 2020.

Hersbach, H., Bell, B., Berrisford, P., Biavati, G., Horányi, A., Sabater, J. M., Nicolas, J., Peubey, C., Radu, R., Rozum, I., Schepers, D., Simmons, A., Soci, C., Dee, D., and Thépaut, J.-N.: ERA5 monthly averaged data on pressure levels from 1940 to present [Dataset], https://doi.org/10.24381/cds.6860a573, 2023.

Huguenin, M. F., Holmes, R. M., and England, M. H.: Drivers and distribution of global ocean heat uptake over the last half century, Nature Communications, 13, 4921, https://doi.org/10.1038/s41467-022-32540-5, 2022.

Irving, D., Hobbs, W., Church, J., and Zika, J.: A Mass and Energy Conservation Analysis of Drift in the CMIP6 Ensemble, Journal of Climate, 34, 3157–3170, https://doi.org/10.1175/jcli-d-20-0281.1, 2020.

Johns, W. E., Elipot, S., Moat, B., Smeed, D. A., King, B., Volkov, D., and Smith, R. H.: Atlantic Meridional Overturning Circulation (AMOC) Heat Transport Time Series between April 2004 and December 2020 at 26.5°N [Dataset], https://doi.org/10.17604/3nfq-va20, 2023.

Kobayashi, S., OTA, Y., HARADA, Y., EBITA, A., MORIYA, M., ONODA, H., ONOGI, K., KAMAHORI, H., KOBAYASHI, C., ENDO, H., MIYAOKA, K., and TAKAHASHI, K.: The JRA-55 Reanalysis: General Specifications and Basic Characteristics, Journal of the Meteorological Society of Japan. Ser. II, 93, 5–48, https://doi.org/10.2151/jmsj.2015-001, 2015.

Large, W. G. and Yeager, S. G.: The global climatology of an interannually varying air–sea flux data set, Climate Dynamics, 33, 341–364, https://doi.org/10.1007/s00382-008-0441-3, 2009.

Li, F., Lozier, M. S., Holliday, N. P., Johns, W. E., Bras, I. A. L., Moat, B. I., Cunningham, S. A., and Jong, M. F. d.: Observation-based estimates of heat and freshwater exchanges from the subtropical North Atlantic to the Arctic, Progress in Oceanography, 197, 102 640, https://doi.org/10.1016/j.pocean.2021.102640, 2021.

https://doi.org/10.5194/essd-2024-545
Preprint. Discussion started: 13 January 2025

Mackay, N., Sohail, T., Zika, J. D., Williams, R. G., Andrews, O., and Watson, A. J.: An optimal transformation method applied to diagnose the ocean carbon budget, Geoscientific Model Development, 17, 5987–6005, https://doi.org/10.5194/gmd-17-5987-2024, 2024.

McDonagh, E. L., King, B. A., Bryden, H. L., Courtois, P., Szuts, Z., Baringer, M., Cunningham, S. A., Atkinson, C., and McCarthy, G.: Continuous Estimate of Atlantic Oceanic Freshwater Flux at 26.5°N, Journal of Climate, 28, 8888–8906, https://doi.org/10.1175/jcli-d-14-00519.1, 2015.

Mecking, J. V. and Drijfhout, S. S.: The decrease in ocean heat transport in response to global warming, Nature Climate Change, 13, 1229–1236, https://doi.org/10.1038/s41558-023-01829-8, 2023.

Moat, B., Smeed, D., Rayner, D., Johns, W. E., Smith, R., Volkov, D., Baringer, M. O., and Collins, J.: Atlantic meridional overturning circulation observed by the RAPID-MOCHA-WBTS (RAPID-Meridional Overturning Circulation and Heatflux Array-Western Boundary Time Series) array at 26N from 2004 to 2022 (v2022.1), British Oceanographic Data Centre - Natural Environment Research Council, UK., https://doi.org/10.5285/04c79ece-3186-349a-e063-6c86abc0158c, 2022.

Nurser, A. J. G., Griffies, S. M., Zika, J. D., and Stanley, G. J.: Mathematics of circulation in arbitrary fluid property spaces, https://doi.org/10.1002/essoar.10511370.2.

Roberts, C. D., Palmer, M. D., Allan, R. P., Desbruyeres, D., Hyder, P., Liu, C., and Smith, D.: Surface flux and ocean heat transport convergence contributions to seasonal and interannual variations of ocean heat content, Journal of Geophysical Research: Oceans, 122, 726–744, https://doi.org/10.1002/2016jc012278, in all locations, except regions of deep convection and water mass transformation, interannual variations in total HC are dominated by the internal rearrangement of heat by ocean dynamics rather than the loss or addition of heat at the surface., 2017.

Schuckmann, K. v., Cheng, L., Palmer, M. D., Hansen, J., Tassone, C., Aich, V., Adusumilli, S., Beltrami, H., Boyer, T., Cuesta-Valero, F. J., Desbruyères, D., Domingues, C., García-García, A., Gentine, P., Gilson, J., Gorfer, M., Haimberger, L., Ishii, M., Johnson, G. C., Killick, R., King, B. A., Kirchengast, G., Kolodziejczyk, N., Lyman, J., Marzeion, B., Mayer, M., Monier, M., Monselesan, D. P., Purkey, S., Roemmich, D., Schweiger, A., Seneviratne, S. I., Shepherd, A., Slater, D. A., Steiner, A. K., Straneo, F., Timmermans, M.-L., and Wijffels, S. E.: Heat stored in the Earth system: where does the energy go?, Earth System Science Data, 12, 2013–2041, https://doi.org/10.5194/essd-12-2013-2020, 2020.

Skliris, N., Zika, J. D., Nurser, G., Josey, S. A., and Marsh, R.: Global water cycle amplifying at less than the Clausius-Clapeyron rate, Scientific Reports, 6, 38 752, https://doi.org/10.1038/srep38752, 2016.

Sohail, T. and Zika, J. D.: Adjusted ERA5, COREv2 and JRA-55 products constrained by ocean observations [Dataset], https://doi.org/10.5281/zenodo.14004937, 2024.

Sohail, T., Zika, J. D., Irving, D. B., and Church, J. A.: Observed poleward freshwater transport since 1970, Nature, 602, 617–622, https://doi.org/10.1038/s41586-021-04370-w, 2022.

Sohail, T., Holmes, R. M., and Zika, J. D.: Watermass Co-Ordinates Isolate the Historical Ocean Warming Signal, Journal of Climate, pp. 1–40, https://doi.org/10.1175/jcli-d-22-0363.1, 2023.

Stocker, T. F.: Chapter 1 The Ocean as a Component of the Climate System, International Geophysics, 103, 3–30, https://doi.org/10.1016/b978-0-12-391851-2.00001-5, 2013.

Talley, L. D.: Freshwater transport estimates and the global overturning circulation: Shallow, deep and throughflow components, Progress in Oceanography, 78, 257–303, https://doi.org/10.1016/j.pocean.2008.05.001, 2008.

https://doi.org/10.5194/essd-2024-545
Preprint. Discussion started: 13 January 2025

Todd, A., Zanna, L., Couldrey, M., Gregory, J., Wu, Q., Church, J. A., Farneti, R., Navarro-Labastida, R., Lyu, K., Saenko, O., Yang, D., and Zhang, X.: Ocean-Only FAFMIP: Understanding Regional Patterns of Ocean Heat Content and Dynamic Sea Level Change, Journal of Advances in Modeling Earth Systems, 12, https://doi.org/10.1029/2019ms002027, 2020.

Trenberth, K. E.: Atmospheric Reanalyses: A Major Resource for Ocean Product Development and Modeling, Proceedings of OceanObs'09: Sustained Ocean Observations and Information for Society, pp. 979–986, https://doi.org/10.5270/oceanobs09.cwp.90, 2010.

Trenberth, K. E. and Caron, J. M.: Estimates of Meridional Atmosphere and Ocean Heat Transports, Journal of Climate, 14, 3433–3443, https://doi.org/10.1175/1520-0442(2001)014<3433:eomaao>2.0.co;2, 2001.

Trenberth, K. E. and Fasullo, J. T.: Atlantic meridional heat transports computed from balancing Earth's energy locally, Geophysical Research Letters, 44, 1919–1927, https://doi.org/10.1002/2016gl072475, 2017.

Trenberth, K. E., Smith, L., Qian, T., Dai, A., and Fasullo, J.: Estimates of the Global Water Budget and Its Annual Cycle Using Observational and Model Data, Journal of Hydrometeorology, 8, 758–769, https://doi.org/10.1175/jhm600.1, 2007.

Trenberth, K. E., Zhang, Y., Fasullo, J. T., and Cheng, L.: Observation-Based Estimates of Global and Basin Ocean Meridional Heat Transport Time Series Observation-Based Estimates of Global and Basin Ocean Meridional Heat Transport Time Series, Journal of Climate, 32, 4567–4583, https://doi.org/10.1175/jcli-d-18-0872.1, 2019.

Tsujino, H., Urakawa, S., Nakano, H., Small, R. J., Kim, W. M., Yeager, S. G., Danabasoglu, G., Suzuki, T., Bamber, J. L., Bentsen, M., Böning, C. W., Bozec, A., Chassignet, E. P., Curchitser, E., Dias, F. B., Durack, P. J., Griffies, S. M., Harada, Y., Ilicak, M., Josey, S. A., Kobayashi, C., Kobayashi, S., Komuro, Y., Large, W. G., Sommer, J. L., Marsland, S. J., Masina, S., Scheinert, M., Tomita, H., Valdivieso, M., and Yamazaki, D.: JRA-55 based surface dataset for driving ocean–sea-ice models (JRA55-do), Ocean Modelling, 130, 79–139, https://doi.org/10.1016/j.ocemod.2018.07.002, 2018.

Valdivieso, M., Haines, K., Zuo, H., and Lea, D.: Freshwater and heat transports from global ocean synthesis, Journal of Geophysical Research: Oceans, 119, 394–409, https://doi.org/10.1002/2013jc009357, 2014.

Valdivieso, M., Haines, K., Balmaseda, M., Chang, Y.-S., Drevillon, M., Ferry, N., Fujii, Y., Köhl, A., Storto, A., Toyoda, T., Wang, X., Waters, J., Xue, Y., Yin, Y., Barnier, B., Hernandez, F., Kumar, A., Lee, T., Masina, S., and Peterson, K. A.: An assessment of air–sea heat fluxes from ocean and coupled reanalyses, Climate Dynamics, 49, 983–1008, https://doi.org/10.1007/s00382-015-2843-3, 2017.

Wunsch, C.: The North Atlantic general circulation west of 50°W determined by inverse methods, Reviews of Geophysics, 16, 583–620, https://doi.org/10.1029/rg016i004p00583, 1978.

Yeager, S. G. and Large, W. G.: CORE.2 Global Air-Sea Flux Dataset [Dataset], https://doi.org/10.5065/D6WH2N0S, 2008.

Zanna, L., Khatiwala, S., Gregory, J. M., Ison, J., and Heimbach, P.: Global reconstruction of historical ocean heat storage and transport, Proceedings of the National Academy of Sciences, 116, 1126–1131, https://doi.org/10.1073/pnas.1808838115, zanna also contributes OH tendency to redistribution, unable to specify the processes that may be contributing to differences in storage., 2019.

Zika, J. D. and Sohail, T.: An optimal transformation method for inferring ocean tracer sources and sinks, EGUsphere, 2023, 1–25, https://doi.org/10.5194/egusphere-2023-1220, 2023.

Zika, J. D. and Sohail, T.: An Optimal Transformation Method for inferring tracer sources and sinks [Dataset], doi.org/10.5281/zenodo.8008629, 2024.

Zika, J. D., Gregory, J. M., McDonagh, E. L., Marzocchi, A., and Clément, L.: Recent Water Mass Changes Reveal Mechanisms of Ocean Warming, Journal of Climate, 34, 3461–3479, https://doi.org/10.1175/jcli-d-20-0355.1, 2021.

https://doi.org/10.5194/essd-2024-545
Preprint. Discussion started: 13 January 2025

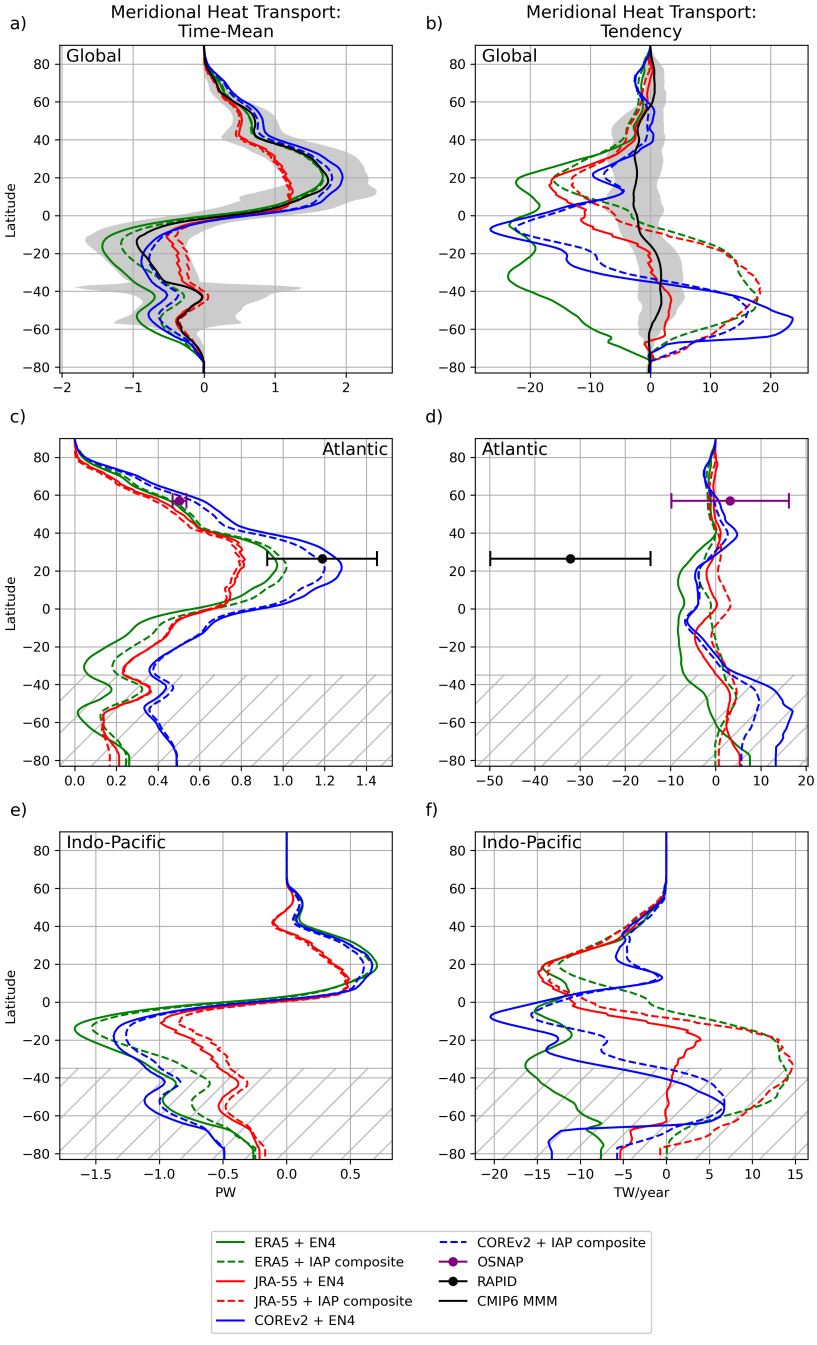

Figure 9. Inferred time-mean meridional heat transport (positive is northward) a) globally, c) in the Atlantic, and e) in the Indo-Pacific. Inferred meridional heat transport tendency b) globally, d) in the Atlantic, and f) in the Indo-Pacific. The CMIP6 multi-model mean is shown by the black line for the global ocean, with one inter-model standard deviation shaded in grey (a and b). RAPID-based estimates are shown by the black dot and whiskers and OSNAP-based estimates are shown by the purple dot and whiskers (c and d).

https://doi.org/10.5194/essd-2024-545
Preprint. Discussion started: 13 January 2025

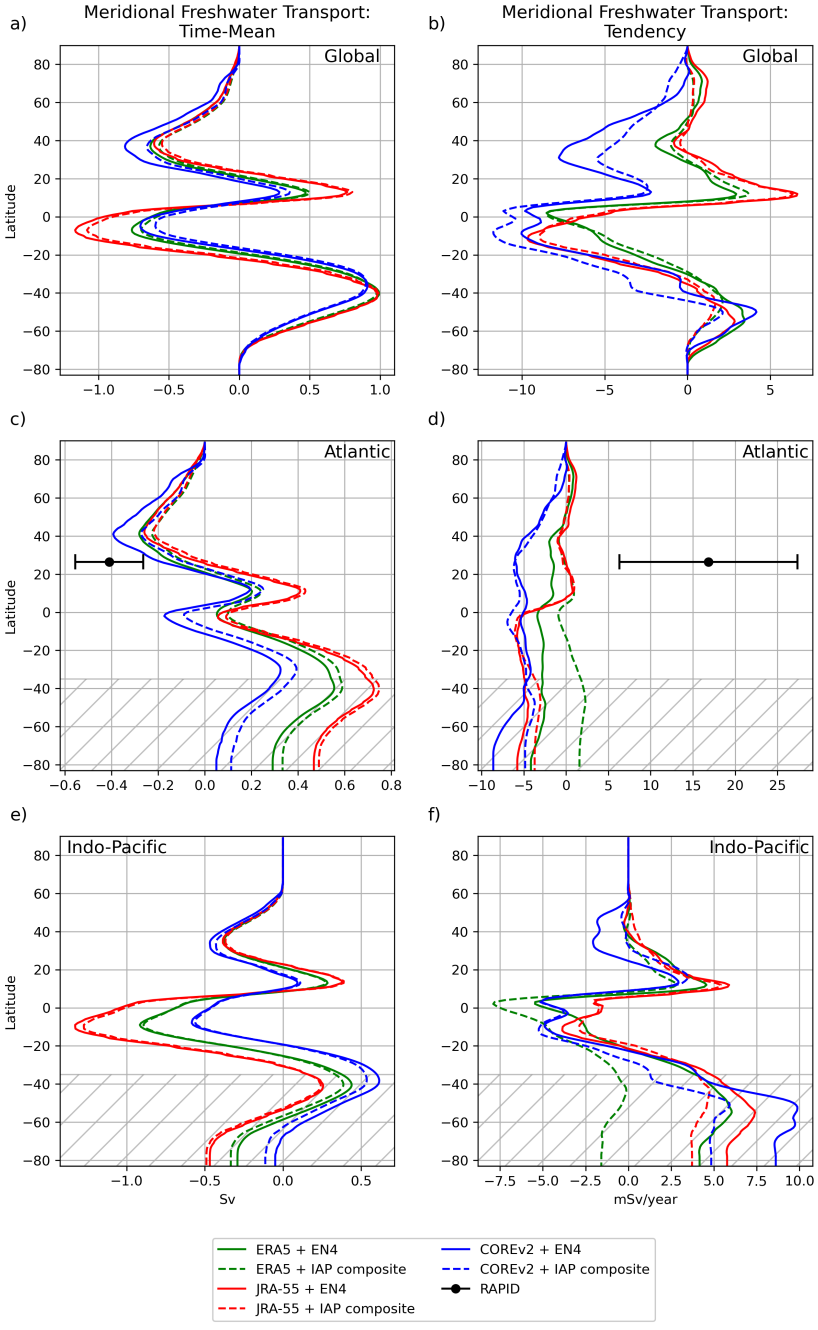

Figure 10. Inferred time-mean meridional freshwater transport (positive is northward) a) globally, c) in the Atlantic, and e) in the Indo-Pacific. Inferred meridional freshwater transport tendency b) globally, d) in the Atlantic, and f) in the Indo-Pacific.